EFFECT OF NO_2 AND NO_3^-/HNO_3 ADSORPTION ON NO PHOTOCATALYTIC CONVERSION

J. Araña*, D. Garzón Sousa*, O. González Díaz, E. Pulido Melián and J. M. Doña Rodríguez

CIDIA-FEAM (Unidad Asociada al Consejo Superior de Investigaciones Científicas, CSIC, avalada por el Instituto de Ciencia de Materiales de Sevilla-Universidad de Sevilla). Instituto de Estudios Ambientales y Recursos Naturales (i-UNAT). Universidad de Las Palmas de Gran Canaria. Edificio del Parque Científico Tecnológico de la ULPGC. Campus de Tafira, 35017-Las Palmas de Gran Canaria, Spain.

Abstract

A study was undertaken of the adsorption and photocatalytic conversion of NO, NO_2 and NO_3^-/HNO_3 using two photocatalysts (P25 and HT-ET). The HT-ET is a catalyst synthesized in our laboratory comprised only of anatase phase and with a surface area three times larger than that of the P25. In powder form, the catalyst was introduced into and extended along the length of a tube with no type of compaction on the part of the solid (pressure drops are negligible under these conditions). This tubular photoreactor arrangement operates as a continuous reactor system enabling FTIR analysis of the surface of the catalysts during the conversion process. NO adsorption was negligible, though the FTIR studies revealed the formation of nitrites on the surface after 18 h of reaction. Overall NO conversion efficiency rates were above 68% with both catalysts in that reaction time. However, selectivity to NO_2 was very high with both catalysts. It was also found with both catalysts that the number of NOx moles eliminated during NO photocatalytic conversion coincided with the number of adsorbed NO_2 moles observed in the adsorption studies performed with this molecule, indicating that the NO_2 molecule is not efficiently converted photocatalytically.

It was observed that most of the NO_2 undergoes disproportionation on the surface of the catalysts, giving rise to nitrates and NO. The FTIR studies showed that a significant proportion of the NO_2 interacts with surface nitrates resulting in $[(NO_3^-)\text{-}(H_2O)_n\text{-}NO_2]$ complexes which are stable on the catalyst surface in an NO atmosphere.

Keywords: TiO_2, NO, NO_2, NOx, photocatalysis, FTIR, nitrates.

*To whom correspondence should be sent

1. Introduction

There has been growing concern over recent decades about the increasing emission of gaseous pollutants into the atmosphere, including volatile organic compounds (VOCs), SOx, NOx, etc. The VOCs and NOx, in particular, have generated emergency situations in some cities where air quality limits have been exceeded. There are two principal methods to control NOx, namely modification of the conditions of combustion processes to reduce their formation or treatment of the effluents [1-3]. The techniques that have been developed to date for effluent treatment include physical adsorption process with alkalis or acids [4, 5], adsorption with sieves, active carbon or metal oxides [6-10] and NOx oxidation or reduction by means of catalysts [11, 12].

Among the oxidation processes are the so-called Advanced Oxidation Treatments (AOTs), with heterogeneous photocatalysis playing a prominent role. The photocatalytic conversion of NO has been widely studied in recent years. This molecule has been used as a probe molecule in numerous studies to test the photocatalytic efficiency of different photocatalysts. The proposed simplified NO photocatalytic conversion process can be summarised in the following stages [13, 14]:

$$NO_{(g)} \xrightarrow[\text{Air} + H_2O_{(g)}]{TiO_{2(s)}+h\nu} NO_{2(g)} \xrightarrow[\text{Air} + H_2O_{(g)}]{TiO_{2(s)}+h\nu} NO^{-}_{3(ads)}$$

Semiconductors have thus been evaluated according to the photocatalytic oxidation selectivity of NO to NO_2 or of NO to NO_3^-, considering the more efficient catalysts to be those which attain higher selectivity to NO_3^-. It should be noted that NO_2 is significantly more toxic than NO [15]. Studies have been performed doping the TiO_2 with Pd, for example, and have shown that this metal enhances selectivity of the photocatalytic conversion of NO to NO_3^- on Pd islands which are poisoned with nitrates [16]. The effect of different exposed crystalline faces of the TiO_2 has also been studied, with results revealing that catalysts with greater exposure of the (001) face, where the photocatalytic oxidation reactions predominate, produce more NO_2 [17]. Studies have even been performed incorporating TiO_2 in construction materials [18], carbon nanotubes [19] or zeolites [20], with the main purpose of their incorporation in many research studies being to avoid or reduce catalyst deactivation. Different studies have

indicated that nitric acid or nitrates, generated as final products of NO photocatalytic conversion, block the photoactive centres, with the TiO_2 being thus deactivated [21-23].

The efficiency of NO photocatalytic conversion has therefore been demonstrated in numerous studies, but important deactivation processes have also been detected [21-23]. Fourier Transform Infrared Spectroscopy (FTIR) studies have been undertaken of the interaction of NO and NO_2 in closed cells with a view to determining the conversion processes and mechanisms [24-27]. However, these FTIR studies were performed under conditions significantly different to the conversion processes. The photocatalytic conversion studies have generally been performed with the catalyst supported on borosilicate glass plates, which complicates an FTIR spectrophotometric analysis of the catalyst surface.

Given this, the present study considers the photocatalytic conversion of NO and NO_2 with incorporation of the photocatalyst in powder form in the interior of a continuously operating tubular reactor and with the semiconductor extended over the whole internal surface of the tube, forming an uncompacted bed. The system can be regarded as a piston-flow tubular reactor in which pressure drops can be considered negligible. The photocatalyst bed on the internal wall of the tube remained stable throughout the tests. In addition to studying the efficiency rate in pollutant elimination and selectivity, it was in this way also possible to study the evolution of the species present on the surface. To avoid dispersal of the catalyst in powder form, the flow rates of the pollutants, dissolved in air with ambient humidity, were lower than those normally used with supported catalysts. These studies were performed with P25, the most commonly used catalyst in NO photocatalytic conversion studies, and a catalyst named HT-ET synthesized in our labs and comprised solely of anatase phase with a surface area three times larger than that of the P25.

2. Experimental

2.1. *Catalysts*

Two catalysts were used, the commercial P25 and the laboratory-synthesised HT-ET. This catalyst was synthesized using the following process:

A mixture of 40 mL of ethanol and 17 mL of titanium tetrabutoxide were added dropwise to a solution of 40 mL of ethanol and 15 mL of water. After this process the mixture was maintained 30 minutes under stirring (1500 rpm). The gel obtained was poured into a Teflon container, bringing it to a total volume of 150 mL with water. This vessel was introduced in a steel autoclave at a pressure of 198.48 kPa, heating it to 423 K during 24 h. Next, the supernatant was removed and the gel was dried at 373 K for another 24 h. The photocatalyst thus obtained was sieved with a 63 μm sieve.

2.2. *Photocatalytic experiments*

The reaction system used is shown in Figure 1. The system is comprised of a borosilicate reactor (photocatalytic reactor) with an external diameter of 8 mm, an internal diameter of 5 mm, length of 150 mm and with two particle filters at the two ends. This photocatalytic reactor is connected to rest of the system via 1/8 copper piping. The photocatalytic reactor output flow is mixed with a 1170 mL/min airflow in the borosilicate mixer shown in Figure 1 before being introduced into the NOx analyser.

The desired concentration of NO_x is obtained by dilution with air of a 100 ppm concentration of NO (supplied by Air Liquide) using mass flow controllers. The NO/air mix is carried out in circuit *A* of the reaction system (Figure 1). Once the desired concentration has been reached in stable form the flow passes to circuit *B* which contains the catalyst in the photocatalytic reactor. In the same way, in circuit *B*, the NO/air mix is maintained until the desired concentration remains stable. Illumination is initiated once stability of the mix had been attained.

Running blanks were also performed to study possible photolysis of the NO and NO_2. While no conversion was observed in the studies with NO, a small conversion below 0.5% took place in the studies with NO_2.

The catalyst (20 mg) was extended in powder form in the reactor. Total workflow was 30 $mL \cdot min^{-1}$ at 1 atm (2.21 $\mu mol \cdot h^{-1}$ of NO) which corresponds to a space-time relationship of 6.7 seconds in the photocatalytic reactor itself and 37.8 seconds when considering the whole reaction system. With the flow rate employed, the catalyst was not displaced at any moment throughout the tests. The tests began after 30 min of adsorption onto the catalyst in darkness and were followed by illumination during 18 h. The light source employed was a 60 W Philips Solarium HB175 lamp equipped with

four 15 W Philips CLEO fluorescent tubes with emission between 300 and 400 nm (λ_{max} = 365 nm, irradiance: 9 mW·cm^{-2}) in the photocatalytic studies. All the studies were carried out at 30 ± 0.5 ºC. Quantification of NO_x was performed using a Horiba APNA-370 N/S analyser. All the tests carried out were performed three times. The maximum errors committed in the analytical determinations are shown in the corresponding figures.

To evaluate the efficiency of the process, the first task was to transform the experimental data of the Horiba analyser, which are expressed in instantaneous concentrations of NO and NO_2 for each reaction time, to molar flows of NO and NO_2, given that the speed of the volumetric flow (flow rate) is known from the mass flow gauges and applying a mass balance to the photoreactor. Once the molar flows had been determined, an integral method was employed over the temporal evolution of the flows to determine, for each reaction time interval, the total number of moles of the species involved. Thus, the number of NO moles introduced in the reactor $\left(NO_{in}\right)$ from time 0 to the time of measurement was estimated through: $\int_0^t F_{NO_{in}} \cdot dt$, the number of NO moles which reacted at each reaction time $\left(NO_{reac}\right)$ was calculated as the difference $\int_0^t F_{NO_{in}} \cdot dt - \int_0^t F_{NO_{out}} \cdot dt$, the number of generated NO_2 moles (NO_2) was calculated as $\int_0^t F_{NO_{2,out}} \cdot dt$ and the number of NO_x moles eliminated during the photocatalytic conversion of NO on the surface, in each period, per gram of photocatalyst, $\left(NO_x\right)_{NO-phot}$, was calculated as:

$$\left(NO_x\right)_{NO-phot}\left(\mu mol \cdot g^{-1}\right) = \frac{\int_0^t F_{NO_{in}} \cdot dt - \int_0^t F_{NO_{out}} \cdot dt - \int_0^t F_{NO_{2,out}} \cdot dt}{w_{cat}}$$

w_{cat} = mass of catalyst in grams.

In the NO_2 adsorption and photocatalytic studies, calculation was also made of the total number of moles introduced in the reactor ($NO_{2,\ in}$) from time 0 to the time of

measurement as $\int_0^t F_{NO_{2,in}} \cdot dt$, the number of NO_2 moles which reacted ($NO_{2,reac}$) as $\int_0^t F_{NO_{2,in}} \cdot dt - \int_0^t F_{NO_{2,out}} \cdot dt$, the number of generated NO moles (NO) as $\int_0^t F_{NO_{out}} \cdot dt - \int_0^t F_{NO_{in}} \cdot dt$ and the number of NO_x moles eliminated in that period during the photocatalytic conversion studies $\left(NO_x\right)_{NO_2-phot}$ or during the adsorption studies $\left(NO_x\right)_{NO_2-ads}$.

The results of the NO conversion studies were expressed as:

- % conversion with respect to the total number of introduced NO moles in each reaction time ($\%NO_{\text{conv}}$) and calculated as:

$$\left(\%NO_{\text{conv}}\right) = 100 \cdot \left[1 - \frac{\int_0^t F_{NO_{out}} \cdot dt}{\int_0^t F_{NO_{in}} \cdot dt}\right]$$

- Selectivity in reference to the production of NO_2 with respect to the total number of converted NO moles, at each instant of the reaction (in the NO photocatalytic conversion studies):

$$\left(S_{NO \to NO_2}\right) = \frac{\int_0^t F_{NO_{2,out}} \cdot dt}{\int_0^t F_{NO_{in}} \cdot dt - \int_0^t F_{NO_{out}} \cdot dt}$$

The results of the NO_2 conversion studies were expressed as:

- Total number of adsorbed NO_2 moles in the tests performed in darkness in a given reaction time, $\left(NO_2\right)_{ads}$ calculated as:

$$\left(NO_2\right)_{ads}\left(\mu\text{mol} \cdot \text{g}^{-1}\right) = \frac{\int_0^t F_{NO_{2,in}} \cdot dt - \int_0^t F_{NO_{2,out}} \cdot dt}{w_{cat}}$$

- Total number of converted NO_2 moles under illumination in a given reaction time $\left(NO_x\right)_{NO_2-phot}$, calculated as:

$$\left(NO_x\right)_{NO_2-phot}\left(\mu\text{mol}\cdot\text{g}^{-1}\right)=\frac{\int_0^t F_{NO_{2,in}}\cdot dt-\int_0^t F_{NO_{2,out}}\cdot dt+\int_0^t F_{NO_{in}}\cdot dt-\int_0^t F_{NO_{out}}\cdot dt}{w_{cat}}$$

- NO formed during disproportionation of NO_2 ($\left(NO\right)_{NO_2-despro}$) was calculated as:

$$\left(NO\right)_{NO_2-disprop}\left(\mu\text{mol}\cdot\text{g}^{-1}\right)=\frac{\int_0^t F_{NO_{out}}dt-\int_0^t F_{NO_{in}}dt}{w_{cat}}$$

The same system was used for the FTIR studies of the interaction of NO or NO_2 with the catlaysts with and without illumination (Figure 1). The spectra that are shown at different reaction times correspond to separate studies. That is, the spectra obtained at 1, 2 and 18 hours of reaction, are separate studies of 1 h, 2 h and 18 h. After this reaction time, the catalyst is removed from the reactor and placed in the CaF_2 cell where the FTIR studies are performed. As previously indicated, each study was performed in triplicate and evolution of the NO and NO_2 was followed using the Horiba analyser. That is, the FTIR interferograms were always obtained *a posteriori* to the photocatalytic tests to see what types of molecule derived from the treated gases (NOx) interact with the photocatalyst surface and what types of modification take place.

2.3 Analysis techniques

Phase composition of the HT-ET was estimated from XRD patterns recorded on a Bruker model D8 Advance diffractometer equipped with a Ni filter and LINXEYE detector using Cu Kα radiation (λ = 1.5418 Å).

BET surface area and pore volume by the Barrett–Joyner–Halenda (BJH) method were determined using N_2 adsorption and desorption isotherms at 77 K measured with a Micromeritics 2010 system.

A Thermo Scientific-Nicolet iS10 spectrophotometer was used for the FTIR studies. The catalyst was placed between two CaF_2 mirrors, and a 4000–1000 cm^{-1} measurement range, 2 cm^{-1} resolution and forward/backward mirror speeds of 10 kHz/6.2 kHz, respectively, were used.

3. Results

3.1 Surface area and phase distribution

Table 1 shows the crystalline phases and surface area of the catalysts used in the study. The P25 has an 80/20 proportion of anatase/rutile phase, whereas the HT-ET only has anatase phase. This latter catalyst has a surface area 3.34 times larger than the P25.

3.2 Characterization of the adsorbed water, hydroxyl groups and surface charge

Figure 2 shows the spectra of the P25 and HT-ET. Note in particular the band attributed to isolated hydroxyl groups (3698 cm^{-1}), the bands attributed to adsorbed water (3600-3000 cm^{-1} and 1640 cm^{-1}) and finally the position of the baseline in each of the catalysts.

The band observed in both catalysts at 1640 cm^{-1} is attributed to the water bending mode (ν_2), while the broad band between 3650 and 3000 cm^{-1} is attributed to antisymmetric (ν_3) and symmetric (ν_1) stretching vibration modes of the water [28, 29]. The intensity of the bands attributed to water in the P25 spectrum is significantly lower than that in the HT-ET spectrum, and is related to the larger surface area of the HT-ET.

As stated above, another important aspect to note in the spectra of Figure 2 is the position of the baseline, which is much higher in the HT-ET than the P25 catalyst. The position of the baseline is related to the presence of surface traps of thermal electrons. Due to the presence of these surface or shallow electron traps (Ti^{3+} type surface defects), electrons are fed to the conduction band via thermal processes such as those generated by the infrared radiation used to obtain the spectra. The electrons promoted to the conduction band have a similar behaviour to that described for delocalised electrons confined to a three-dimension box with infinite walls; the high density of generated states gives rise to the continuous presence of excited electrons leading to a baseline

increase of the infrared spectrum [30, 31]. The results would seem to indicate that the HT-ET catalyst has an important concentration of surface or sub-surface electron traps.

3.3 Photocatalytic conversion of NO

As indicated in the Experimental section, the NO photocatalytic conversion studies were performed continuously with an NO flow of 2.21 μmol·h^{-1}. As also mentioned in section 2.2, two blank reaction tests were performed before commencing each photocatalytic study; one without illumination and without catalyst, and one without illumination but with catalyst. During these blank studies, the formation of NO_2 was not observed from the reaction:

$$2NO + O_2 \longrightarrow 2NO_2 \qquad (1a)$$

Figure 3 shows the evolution over time of the (% NO_{conv}) for the P25 and the HT-ET during the photocatalytic studies. During the first few minutes of the reaction a 100% elimination rate can be seen with both catalysts of all the NO introduced into the system. Subsequently, the efficiencies in NO elimination progressively decrease for both catalysts, reaching values after 18 h of reaction time of 68% and 76% for the P25 and the HT-ET, respectively. It should be noted that the decrease in efficiency is significant in the first six hours of reaction, with the variation in (% NO_{conv}) being very slight after this reaction time.

As indicated in the Experimental section, during the NO conversion studies it was possible to follow the formation of NO_2 against reaction time and calculate the selectivity of NO to NO_2, taking into account the total number of NO moles consumed in relation to the reaction time, and the total number of generated NO_2 moles. Figure 4 shows the evolution over time of selectivity of NO to NO_2 $\left(S_{NO\rightarrow NO_2}\right)$ for both catalysts. During the first 2 h of reaction with the P25, and during the first 4 h of reaction with the HT-ET, the $\left(S_{NO\rightarrow NO_2}\right)$ increases rapidly from 0 to 0.5 in the P25 and from 0 to 0.3 in the HT-ET. After these instants, the $\left(S_{NO\rightarrow NO_2}\right)$ continues to increase during the

subsequent reaction hours but at a significantly slower rate. Though the (% NO_{conv}) is significantly high during the period for both catalysts, over 68%, low $\left(S_{NO\rightarrow NO_2}\right)$ are only attained during the first few reaction hours. In other words, important eliminations of NOx are only obtained in the first few reaction hours.
Very similar efficiencies in the % conversion of NO and selectivity have been obtained in other studies with P25 deposited on different surfaces [19, 32, 33].

3.3.1 FTIR studies of adsorption and photocatalytic conversion of NO

Studies with both catalysts were carried out of NO adsorption using the flows as in the conversion studies and, logically, without irradiation, with no appreciable decreases being observed in the flows at the photoreactor outlet. However, in the analysis of the spectra (Figure 5), the formation of a band was found at 1263 cm^{-1} after 18 h of reaction in the P25 and bands at 1605, 1582, 1471, 1378, 1356, 1294 and 1251 cm^{-1} in the HT-ET. The band observed at 1263 cm^{-1} in the P25 is attributed to the vibration ν_3 of ionic nitrites. The bands observed in the HT-ET will be discussed in subsequent sections.

Spectra were taken at different reaction times during the NO photocatalytic conversion studies indicated in section 3.3 (Figs. 4 and 5). Figure 6 (A and B) shows the FTIR spectra obtained after analysing the P25 (A) and HT-ET (B) surfaces at different reaction times.

In the spectrum obtained after analysis of the surface of the P25 in the region between 2000-1000 cm^{-1} and after 1 h of reaction (Figure 6A), namely after (%NO_{conv}) began to decrease significantly, the formation was observed of a band at 1574 cm^{-1}, a broad band centred at 1435 cm^{-1}, another at 1304 cm^{-1} with a long shoulder, and another at 1264 cm^{-1}. After 2 h of reaction time, the band which was initially found at 1574 cm^{-1} had shifted to 1577 cm^{-1} and the bands which were observed between 1500 and 1300 cm^{-1} were more sharply defined. Finally, in the spectrum obtained after 18 h of reaction, the clear definition was observed of a band at 1610 cm^{-1} which had not been observed in the initial spectra. The band which was initially at 1574 cm^{-1} and at two hours at 1577 cm^{-1} had now shifted to 1587 cm^{-1}. The broad band in the region between 1500 and 1300 cm^{-1} had increased in intensity and the wavenumbers changed to 1448, 1300 and 1264 cm^{-1}.

The spectrum obtained with the HT-ET after 1 h of reaction (Figure 6 B) displayed poorly defined bands similar to those obtained in the NO adsorption studies after 18 h of reaction. At 2 h of reaction time, bands were observed at 1610, 1582, 1300 and 1251 cm^{-1}. Finally, after 18 h of reaction, bands at 1615, 1490 and 1289 cm^{-1} can be seen well defined and with greater intensity. Bands are also observed at this reaction time at 1584 and 1245 cm^{-1}, though with less intensity than those observed in the P25.

The stability of the bands obtained from the sample at 18 h of reaction time was studied in an air-only atmosphere. For this, an analysis was undertaken of the evolution over 12 hours of the bands observed in the spectrum obtained at 18 h of reaction time with NO. Figure 7 shows the evolution over time of the bands with the HT-ET catalyst. As can be seen, the bands at 1615, 1490 and 1289 cm^{-1} progressively decrease in intensity and produce, after 4 h, a spectrum similar to that obtained with the P25 after 18 h of reaction (Figure 6A). The only notable difference can be seen in the position of the broad band, which is found in the HT-ET at 1430 cm^{-1} and in the P25 at 1448 cm^{-1}. After 12 h, a spectrum is obtained formed solely of two almost symmetrical broad bands at 1410 and 1330 cm^{-1} and a small band at 1043 cm^{-1}. It should be noted that the band at 1584 cm^{-1}, which barely changed in intensity during the first 4 h, finally disappeared. The sample obtained with the P25 after 18 h of reaction was subjected to the same process. The spectrum obtained at the end was the same as that obtained with the HT-ET, namely two almost symmetrical broad bands at 1410 and 1330 cm^{-1} and a smaller band at 1043 cm^{-1}. These latter bands are attributed to ν_3 vibrations of solvated nitrates [34]. However, attributing the initial bands is more controversial. These bands have been observed in other studies at very similar wavenumbers and with very similar intensities and have been attributed to asymmetric and symmetric vibrations of mono- and bidentate nitrates [35, 36]. Nonetheless, mono- and bidentate nitrates are characterized as being very stable compounds and once formed, can only be decomposed at elevated temperatures [37]. In the present study, it was observed that these bands, in the absence of illumination and in an NO-free atmosphere, are progressively transformed into the aforementioned ionic nitrates. On the other hand, nitro-nitrite compounds also display bands in the region between 1650-1300 cm^{-1} depending on the coordination group [38-40]. It has been reported that NO_2 can be adsorbed giving rise to an intense band between 1630-1620 cm^{-1} [41.42]. It has also been reported that NO_2 can react with nitrates, forming complexes which give rise to bands in the 1600 cm^{-1} region [43]. These

types of nitro-compound are stable in an atmosphere of NO and NO + O_2, but decompose in other atmospheres [27, 44]. The final compounds of NO photocatalytic conversion are nitrates and the observed bands correlate very well with those of the reported [(NO_3^-)-$(H_2O)_n$-NO_2] complexes. Thus, the bands at 1491 and 1289 cm^{-1} can tentatively be attributed to the ν_3 (low) and ν_3 (high) vibrations respectively of monodentate nitrates interacting with NO_2 (band at 1615 cm^{-1}) and the bands at 1587 and 1263 cm^{-1} to the ν_3 (low) and ν_3 (high) vibrations, respectively, of bidentate nitrates interacting with NO_2. This would explain the progressive shift observed in the studies with the P25 of the band initially observed at 1574 cm^{-1} and the width of the bands at 1490 and 1300-1289 cm^{-1}. Decomposition of the complexes is faster with the P25, and so in the spectrum obtained after 18 hour of reaction the same bands are observed as in the HT-ET after 4 h in an air-only atmosphere. The slower decomposition of these species with the HT-ET compared to the P25 may be due to the presence of electron traps in the HT-ET. It has been reported that NO activation and decomposition occur on the same centres as those adsorbing oxygen. In fact, the behaviour of the NO molecule is similar in several respects to that of the oxygen molecule [45, 46]. Interaction of the NO with oxygen vacancies where nitrates, mono- and bidentate, which form complexes with the NO_2, may be stabilizing these complexes. However, when the catalyst is extracted from the reactor and the NO atmosphere is lost, the oxygen must displace it from these centres giving rise to the decomposition of the complexes observed in Figure 7.

3.4 Adsorption and photocatalytic conversion studies of NO_2

The first intermediate in the photocatalytic conversion of NO is NO_2. In the previous section it was observed how this molecule intervenes in the formation of complexes with surface nitrates. The NO_2 displays an important capacity for adsorption and disproportionation on the surface of different materials [35, 47, 48]. In addition, some studies have reported that photocatalytic conversion of the NO_2 to nitrates may be the limiting stage of the process or not very efficient [19, 49]. The disproportionation reactions of the adsorbed NO_2 may be taking place with surface oxygen ions [50], or the water or surface hydroxyl groups [26, 51].

$$3NO_{2,ads} + O_{br}^{2-} \longrightarrow 2NO_{3,ads}^{-} + NO_{(g)} \quad (1b)$$

$$2NO_{2,ads} + H_2O_{(ads)} \longrightarrow HONO_{(ads)} + HNO_{3,ads} \quad (2b)$$

$$NO_{2,ads} + HONO_{(ads)} \longleftrightarrow HNO_{3,ads} + NO_{(g)} \quad (3b)$$

$$3NO_{2,ads} + 2OH_{ads}^{-} \longrightarrow 2NO_{3,ads}^{-} + NO_{(g)} + H_2O_{(ads)} \quad (4b)$$

Taking into consideration these aspects, the photocatalytic conversion was studied of an NO_2-NO mix (with initial flows of 1.79 μmol·h^{-1} and 0.12 μmol·h^{-1} of NO_2 and NO, respectively). The NO was incorporated in the reaction mix to simulate similar conditions to those of the NO conversion studies given that it has been observed (section 3.3.1) that an NO atmosphere facilitates formation of the reported complexes. As in the studies with NO, the NO_2-NO mix with air is carried out in circuit *A* of the reaction system (Figure 1). When the desired concentration is attained in stable form, it is passed through circuit *B* which contains the catalyst to carry out the adsorption studies. These studies were undertaken, with and without illumination, with a view to determining the effect that NO_2 adsorption has on the process. Figure 8 (A and B) shows the results for the two catalysts of the evolution over time of the total number of adsorbed NO_2 moles per gram of catalyst, $(NO_2)_{ads}$ obtained from the studies in darkness. Figure 8 also shows the evolution over time of the total number of converted NO_2 moles, $(NO_x)_{NO_2-phot}$, obtained from the photocatalytic conversion studies performed under illumination with the two catalysts. Also shown in these figures, for purposes of comparison, is the evolution over time of the total number of NO_x moles eliminated during the photocatalytic conversion of the NO, $(NO_x)_{NO-phot}$ whose results were indicated in the previous section (Figure 4). The equations used for the calculation of the total number of moles at each reaction time have been indicated in section 2.2.

As can be seen, the behaviour of the molar profile for $(NO_2)_{ads}$ is the same, with both catalysts, to that which corresponds to $(NO_x)_{NO_2-phot}$ and to $(NO_x)_{NO-phot}$ during the first 6 h of reaction. After this reaction time, the molar profile of the $(NO_2)_{ads}$ is higher than the $(NO_x)_{NO_2-phot}$ and the $(NO_x)_{NO-phot}$. However, in other studies in which NO_2 adsorption has been studied, without the presence of NO in the flow, adsorption of this molecule was significantly lower than photocatalytically converted NO_2 [19]. With the

P25 and the HT-ET, a slowing down takes place of NO_2 elimination under illumination at 6 and 12 h of reaction respectively. A lower elimination of NO_2 is observed with both catalysts in the NO_2 photocatalytic conversion studies than in the adsorption studies (Figure 8).

Also shown (see Figure 8) is the $(NO_x)_{NO_2-phot}$ namely the total number of NO_x moles eliminated during photocatalytic conversion of the NO with both catalysts. As can be seen, the $(NO_x)_{NO-phot}$ is always lower than $(NO_2)_{ads}$ and practically the same as $(NO_x)_{NO_2-phot}$. These results indicate that NO_2 is not efficiently photocatalytically converted.

The values of the $(NO_2)_{ads}$, $(NO_x)_{NO_2-phot}$ and $(NO_x)_{NO-phot}$ with the HT-ET are almost twice as high as those obtained with the P25, which could be attributed to the larger surface area of the HT-ET.

While the formation of NO was observed during the NO_2 adsorption studies, it was barely detected during the photocatalytic studies. As was mentioned in section 2.2, a small proportion (< 0.5%) of NO_2 is photolytically decomposed. Given that NO concentrations are barely detected during the NO_2 photocatalytic studies, this would seem to indicate that NO_2 adsorption does not inhibit photocatalytic conversion of the NO added or generated as the result of disproportionation of the NO_2 or photolysis of this molecule.

According to reactions (1b-4b), one molecule of NO is produced for each 3 disproportionated molecules of NO_2. Figure 9 shows the evolution over time of the total number of NO moles formed during the adsorption reaction time, $(NO)_{despro\rightarrow NO_2}$, the product of $\left[(NO)_{disprop\rightarrow NO_2}\times 3\right]$ in order to evaluate the number of NO_2 moles consumed in the disproportionation, and the remainder from $(NO_2)_{ads}-\left[(NO)_{disprop\rightarrow NO_2}\times 3\right]$ in order to evaluate the number of NO_2 moles which do not undergo disproportionation via reactions (1a-4a). As can be seen, after 6 h with the P25 and 12 h with the HT-ET, the NO_2 stops producing NO and, therefore, disproportionation of the NO_2 ceases. However, the NO_2 continues to be adsorbed, and

with a linear increase. $(NO)_{disprop \rightarrow NO_2}$ decreases in the P25 when NO_2 disproportionation stops. This could indicate reactions between NO and adsorbed species.

3.5 FTIR studies during the adsorption and photocatalytic conversion of NO_2

Figure 10 shows the spectra obtained after 18 h of reaction of the NO_2 with the P25 and HT-ET with and without illumination. Also shown in Figure 10 for purposes of comparison is the spectrum obtained after 18 h in the NO photocatalytic studies. The spectra obtained with both catalysts of NO_2 photocatalytic conversion are practically identical to those obtained during the NO photocatalytic conversion with bands at 1614, 1585, 1490, 1290 and 1249 cm^{-1} in the HT-ET and bands at 1610, 1587, 1448, 1300 and 1264 cm^{-1} in the P25. In the spectra obtained of NO_2 adsorption, the band at 1614 cm^{-1} is of significantly lower intensity while the bands between 1300 and 1400 cm^{-1} are of greater intensity. These catalysts with the adsorbed species were left for 12 h in darkness. In all cases, the elimination was observed of the aforementioned bands as well as the formation of ionic nitrates, as was also observed in the studies performed with the species generated from the photocatalytic conversion of NO.

3.6 Photocatalytic conversion studies of HNO_3 and NO_3^-

In all the NO photocatalytic studies it was observed that the final product is HNO_3 or NO_3^-. Some studies report that as a consequence of the presence of HNO_3 on the catalyst surface the photocatalytic conversion of NO results only in NO_2 [52]. Most of the photocatalytic studies undertaken to date report that the nitric acid and/or nitrates generated and adsorbed on the surface are responsible for deactivation of the semiconductors as they block the available photoactive centres [53-55]. To avoid this, studies have been carried out using nitric acid adsorbents as zeolites [20]. In the studies of the present work described in the previous section, it was observed that the NO_2 is not efficiently photocatalytically converted but rather undergoes disproportionation on being adsorbed, giving rise to NO and nitrates. The FTIR analysis of the adsorbed species revealed the formation on the surface of the catalysts of NO_2-nitrates complexes that, in the absence of an NO atmosphere, evolve into ionic nitrates. For this reason, and with a view to a more profound study of these species, it was decided in the present

work to also perform NO photocatalytic studies with the presence of HNO_3 and/or NO_3^- adsorbed on the catalyst surface. Though these studies were performed with both catalysts, only those for the P25 are shown as the results for both catalysts were similar. Firstly, a study was made of HNO_3 photolysis. The catalyst was impregnated with HNO_3 with a flow of 361 µmol/min during 15 min. Figure 11 A shows the total number of NO_2 moles produced against reaction time. The results clearly show the occurrence of HNO_3 photolysis. It has also been reported that the adsorbed HNO_3 is photolytically decomposed [56].

A study was also performed of the reaction of the NO with the HNO_3 adsorbed on the catalyst surface without illumination (Figure 11 B). A progressive increase can be seen of the % elimination of the introduced NO over the first 0.2 h, reaching 60% at that time without NO_2 formation. Beyond this reaction time, the % elimination of NO remained constant for the next 0.4 h before progressively declining. After 0.2 h of reaction time, the progressive formation of NO_2 can also be observed, and after 0.4 h until the end of the study a selectivity rate of 2 of NO to NO_2 was maintained. In other words, 2 NO_2 molecules were formed for each eliminated NO molecule. The following reactions have been proposed in different studies which may explain the observations made in the present study [57, 58]:

$$HNO_{3,ads} + NO_{(g,ads)} \longrightarrow NO_{2,(g)} + HONO_{(ads)} \quad (1c)$$

$$HNO_{3,ads} + HONO_{(ads)} \longrightarrow 2NO_{2,(g)} + H_2O_{(ads)} \quad (2c)$$

$$H^+_{ads} + NO^-_{3,ads} \longleftrightarrow \text{Complex} \quad (1d)$$

$$\text{Complex} + NO_{ads,(g)} \longrightarrow HNO_{2,ads} + NO_{2,ads(g)} \quad (2d)$$

$$2HNO_{2,ads} \longrightarrow NO_{(g)} + NO_{2,(g)} + H_2O_{ads} \quad (3d)$$

$$NO^-_{3,ads} + O^{2-}_{br} + 2NO_{g,ads} \longrightarrow 3NO^-_{2,ads} \quad (4d)$$

$$NO^-_{3,ads} + 2NO_{g,ads} \longrightarrow NO^+_{ads} + 2NO^-_{2,ads} \quad (5d)$$

$$NO^-_{3,ads} + 2NO_{g,ads} \longrightarrow N_2O_{3,ads} + NO^-_{2,ads} \quad (6d)$$

These reactions also explain the decrease in $(NO)_{disprop\rightarrow NO_2}$, after the first 6 hours of reaction, in the adsorption studies with P25 (Figure 9 A).

A study was also made of the species generated during this process (Figure 12). In the initial spectrum obtained of interaction of the HNO_3 with the P25 surface, a shoulder can be seen in the δOH water vibration band over 1658 cm^{-1} and bands at 1577, 1427, 1325 and 1310 cm^{-1}. The bands at 1658 and 1310 cm^{-1} are attributed to adsorbed molecular HNO_3, the bands at 1423 and 1320 cm^{-1} to ionic nitrates [34] and the band observed at 1577 cm^{-1} to bidentate nitrates, which is similar to that observed in the P25 during the first hour of reaction [35, 36]. After the study with NO, the same bands were observed as those obtained in the NO and NO_2 photocatalytic studies. The sample, after the studies with NO, was analysed at different times and it was observed how the bands evolved, as in the previous studies, to the formation of ionic nitrates (bands at 1423 and 1340 cm^{-1}). The same studies were repeated with the adsorbed HNO_3 but passing a same flow of NO_2 as that used in the NO tests, with the same spectrum being obtained. Therefore, it would appear that the bands observed at 1615, 1585, 1435(1480) and 1300 cm^{-1} are due to $[(NO_3^-)\text{-}(H_2O)_n\text{-}NO_2]$ complexes, as indicated above. A higher relative intensity of the band at 1614 cm^{-1} was observed in the FTIR studies performed with NO and NO_2 under illumination. It has been reported that adsorbed nitrates have a high capacity to be hydrated, with this capacity being higher in monodentate than bidentate nitrates. It has also been reported that NO_2 interacts with base centres like the hydroxyl groups [26].

4. Discussion

The photocatalytic conversion process of NO has been described through three possible mechanisms [59]:

I) Oxidation with $^{\bullet}OH$ radicals

$$TiO_2 + h\nu \rightarrow TiO_2\left(h^+ + e^-\right) \quad (1e)$$

$$TiO_2\left(h^+\right) + H_2O_{ads} \rightarrow TiO_2 + {}^{\bullet}OH_{ads} + H^+_{ads} \quad (2e)$$

$$TiO_2\left(h^+\right) + OH_{ads} \rightarrow TiO_2 + {}^{\bullet}OH_{ads} \quad (3e)$$

$$TiO_2\left(e^-\right) + O_{2ads} \rightarrow TiO_2 + O^{\bullet-}_{2,ads} \quad (4e)$$

$$NO_{ads} + {}^{\bullet}OH_{ads} \rightarrow HNO_{2,ads} \quad (1f)$$

$$HNO_{2,ads} + {}^{\bullet}OH_{ads} \rightarrow NO_{2,ads} + H_2O_{ads} \quad (2f)$$

$$NO_{2,ads} + {}^{\bullet}OH_{ads} \rightarrow HNO_{3,ads} \leftrightarrow NO^{-}_{3,ads} + H^{+}_{ads} \quad (3f)$$

II) Oxidation with the holes

$$TiO_2\left(h^+\right) + NO_{ads} + H_2O_{ads} \rightarrow HNO_{2,ads} + H^{+}_{ads} \quad (1g)$$

$$TiO_2\left(h^+\right) + HNO_{2,ads} \rightarrow NO_{2,ads} + H^{+}_{ads} \quad (2g)$$

III) Oxidation with bridging oxygen

$$TiO_2\left(h^+, O^{2-}_{br}\right) \rightarrow TiO_2\left(O^{\bullet}_{br}\right) \quad (1h)$$

$$TiO_2\left(O^{\bullet}_{br}\right) + NO_{ads} + H_2O_{ads} \rightarrow TiO_2\left(\square\right) + HNO_{2,ads} + OH^{-}_{ads} \quad (2h)$$

$$TiO_2(O_s\cdot) + HNO_{2ads} \rightarrow TiO_2(O_s) + NO_{2ads} + H^{+} \quad (3h)$$

$$TiO_2\left(O^{\bullet}_{br}\right) + HNO_{2,ads} \rightarrow TiO_2\left(O_{br}\right) + NO^{-}_{2,ads} + H^{+}_{ads} \quad (4h)$$

$$TiO_2\left(O^{\bullet}_{br}\right) + HNO_{2,ads} \rightarrow TiO_2\left(\square\right) + HNO^{-}_{3,ads} \quad (5h)$$

$$TiO_2\left(O_{br}\right) + HNO^{-}_{3,ads} \rightarrow TiO_2\left(O^{\bullet}_{br}\right) + HNO_{3,ads} \quad (6h)$$

$$TiO_2(O_s\cdot) + HNO_3^{-}{}_{ads} \rightarrow TiO_2(O_s\cdot) + HNO_{3ads} \quad (7h)$$

$$TiO_2\left(O^{\bullet}_{br}\right) + NO_{2,ads} + H_2O_{ads} \rightarrow TiO_2\left(\square\right) + HNO_{3,ads} + OH^{-}_{ads} \quad (8h)$$

$$TiO_2\left(O^{\bullet}_{br}\right) + NO_{2,ads} \rightarrow TiO_2\left(\square\right) + NO^{-}_{3,ads} \quad (9h)$$

However, in many studies the reaction of NO with $O^{\bullet-}_2$ radicals is not taken into account:

IV) Oxidation by means of the $O^{\bullet-}_2$ radical

$$NO_{ads} + O^{\bullet-}_{2,ads} \rightarrow ONOO^{-}_{ads} \quad (1i)$$

$$NO_{2,ads} + O^{\bullet-}_2 \rightarrow O_2NOO^{-}_{ads} \quad (2i)$$

Different decomposition processes of the peroxynitrite and peroxynitrate have been reported [60]:

$$ONOO^-_{ads} \leftrightarrow \left[ONO^{\bullet} - O^{\bullet -}\right]^{\#}_{ads} \leftrightarrow NO_{2,ads} + O^{\bullet -}_{ads} \quad (3i)$$

$$\left[ONOOH\right]_{ads} \rightarrow NO_{2,ads} + {}^{\bullet}OH_{ads} \quad (4i)$$

$$ONOO^-_{ads} \rightarrow NO^-_{ads} + O_{2,ads} \quad (5i)$$

$$O_2NOO^-_{ads} \rightarrow NO^-_{2,ads} + O_{2,ads} \quad (6i)$$

It should be borne in mind that, for oxidation of NO to HNO_3/NO_3^- by means of mechanisms I-III, the generation of 3 holes (h^+) is necessary, and that, during the formation of these three holes, 3 $O_2^{\cdot -}$ radicals are formed. Therefore, for each NO molecule that is converted via mechanisms I-III, three NO molecules are converted via the $O_2^{\bullet -}$ radicals.

The conversion of NO to NO_2 can also take place naturally through reaction (1a). However, as mentioned in section 2.2, this reaction was not observed at any moment in the studies performed without illumination. The natural oxidation process of NO to NO_2 has been described through three different kinetic models [61,62]:

$$2NO + O_2 \rightarrow \left[ONOONO\right]^{\#} \rightarrow 2\,NO_2 \quad (1j)$$

$$NO + NO \rightarrow (NO)_2 \quad (1k)$$

$$(NO)_2 + O_2 \rightarrow 2\,NO_2 \quad (2k)$$

$$NO + O_2 \rightarrow NO_3 \quad (1l)$$

$$NO + NO_3 \rightarrow 2\,NO_2 \quad (2l)$$

All of the three models proposed display a very slow conversion of NO to NO_2 [61, 63]. The low space-time values obtained in the reaction conditions employed in the present study, the low NO concentration values tested and the dynamic conditions are the main reasons why this reaction does not take place.

It has been shown in the present work that the number of NO_x moles eliminated during the photocatalytic conversion of NO and NO_2 coincides or is lower than the number of adsorbed or disproportionated NO_2 moles determined in the studies with NO_2/NO mixes

(section 3.4). According to the results, 56.7% of adsorbed NO_2 with the P25 undergoes disproportionation producing NO, and 87.12% with the HT-ET. The rest of the NO_2 is adsorbed without disproportionation, with no efficient photocatalytic conversion of NO_2 being observed. The FTIR studies revealed bands which, in an NO-free atmosphere, evolve into ionic nitrates and which are attributed to $[(NO_3^-)\text{-}(H_2O)_n\text{-}NO_2]$ complexes. The % of NO_2 which does not undergo disproportionation, as observed in the NO_2 adsorption studies, may be due to formation of these complexes. It was also observed with both catalysts that the NO_2 eliminated in the NO_2 adsorption studies was higher than that eliminated in the NO_2 photocatalytic studies. In the studies with NO_2 + irradiation the formation of NO was not observed as NO is photocatalytically converted through reactions (2h and 3h), reacting with the surface O^{2-} (bridging oxygen). It was observed in the FTIR studies that the stability of the $[(NO_3^-)\text{-}(H_2O)_n\text{-}NO_2]$ complexes depends on the presence of an NO atmosphere. The absence of such an atmosphere and the competition for bridging oxygen because of the photocatalytic conversion of the NO may be the cause of the lower NO_2 adsorption under illumination than in darkness. Interaction of NO with oxygen vacancies may be stabilizing the $[(NO_3^-)\text{-}(H_2O)_n\text{-}NO_2]$ complexes. It has been reported that NO competes with oxygen for adsorption centres/oxygen vacancies [45, 46].

It has also been shown in the present work that adsorbed HNO_3 photolytically decomposes to NO_2, and that NO reacts with HNO_3 and/or $NO_3^-\text{-}H^+$ giving rise to NO_2. Therefore, reactions (3f) and (7h) do not take place, or of minimal importance. The photolytic decomposition of adsorbed HNO_3, or the reaction of NO/NO_2 with NO_3^-, could explain why the photocatalytic conversion of NO_2 is not effective, with the adsorption and disproportionation processes of this molecule being favoured. It is confirmed that NO is photocatalytically converted to NO_2 and that the efficiency of this reaction falls only to 32% with the P25 and 25% with the HT-ET after 18 h of reaction. The NO_2 that is generated is eliminated from the outlet flow via its disproportionation and/or its reaction with surface nitrates forming $[(NO_3^-)\text{-}(H_2O)_n\text{-}NO_2]$ complexes. The centres where the NO_2 undergoes disproportionation may be responsible for the reduction in the efficiency of NO photocatalytic elimination. This is seen in the fact that the values of $\left(NO_x\right)_{NO-phot}$ are the same as those for $\left(NO_2\right)_{ads}$ and $\left(NO_x\right)_{NO_2-phot}$ during the first 6 h of reaction in which NO_2 disproportionation takes place producing NO. At

longer reaction times, the profiles of $(NO_x)_{NO-phot}$ and $(NO_x)_{NO_2-phot}$ are lower than that of $(NO_2)_{ads}$ due to the surface changes that take place because of the formation of oxygen vacancies.

The formation of $[(NO_3^-)\text{-}(H_2O)_n\text{-}NO_2]$ complexes may be inhibiting NO reactions with HNO_3 and/or NO_3^- and favouring, in this way, the final formation of nitrates.

Taking into account these results, the global mechanism of the photocatalytic conversion of NO obtained from the studies carried out in this work is summarized in Figure 13.

4. Conclusions

The reaction system used in the present work, with the catalyst unsupported and in powder form, has given similar results of activity in NO and NOx elimination to those reported in other studies with supported catalysts. Using this system, it has been possible to analyse with FTIR spectroscopy the presence of different species adsorbed on the surface of the catalysts after different reaction times.

A correlation is determined between NO_2 adsorption and NO_x elimination in the photocatalytic conversion of NO and NO_2 using commercial (P25) and laboratory synthesized (HT-ET) catalysts. It is shown that NO_2 is not efficiently photocatalytically converted, but rather is adsorbed undergoing disproportionation. It is also shown that NO_2 interacts with the surface nitrates forming stable $[(NO_3^-)\text{-}(H_2O)_n\text{-}NO_2]$ complexes in an NO atmosphere. In an NO-free atmosphere, these complexes decompose into ionic nitrates. It is also shown that adsorbed HNO_3 photolytically decomposes and that NO reacts with $HNO_3/NO_3^-\text{-}H^+$ giving rise to NO_2. These reactions seem to be inhibited by the formation of $[(NO_3^-)\text{-}(H_2O)_n\text{-}NO_2]$ complexes and appear to be responsible for the non-efficient photocatalytic conversion of NO_2.

The two catalysts used in the study, P25 and HT-ET, show the same behaviour regarding % decrease of NO elimination, increase in selectivity of NO to NO_2, and NO_2 adsorption and disproportionation. The formation of the $[(NO_3^-)\text{-}(H_2O)_n\text{-}NO_2]$ complex was also observed with both catalysts, although the decomposition rate was higher with P25. The larger surface area and the presence of surface electron traps may be behind the slower decomposition rate of these complexes with the HT-ET catalyst.

The results obtained in the present study will enable optimization of the design of treatment systems for the photocatalytic conversion of NO_x.

Bibliography

[1] B. Coda, F. Kluger, D. Förtsch, H. Spliethoff, K. R. G. Hein, LTognotti, Coal-Nitrogen Release and NO_x Evolution in Air-Staged Combustion, Energ Fuel. 12 (1998) 1322–1327.

[2] J. Zhu, Z. Ouyang, Q. Lu, An Experimental Study on NO_x Emissions in Combustion of Pulverized Coal Preheated in a Circulating Fluidized Bed, Energ Fuel. 27 (2013) 7724–7729.

[3] V.V. Lissianski, P. M. Maly, V. M. Zamansky, Utilization of Iron Additives for Advanced Control of NO_x Emissions from Stationary Combustion Sources, Ind. Eng. Chem. Res. 40 (2001) 3287–3293.

[4] D. Thomas, J. Vanderschuren, Modeling of NO_x Absorption into Nitric Acid Solutions Containing Hydrogen Peroxide, Ind. Eng. Chem. Res. 36 (1997) 3315–3322.

[5] C. H. Nelli, G. T. Rochelle, Nitrogen Dioxide Reaction with Alkaline Solids, Ind. Eng. Chem. Res. 35 (1996) 999–1005.

[6] Q. Yu, H. Wang, T. Liu, L. Xiao, X. Jiang, X. Zheng, High-Efficiency Removal of NO_x Using a Combined Adsorption-Discharge Plasma Catalytic Process, Environ. Sci. Technol. 46 (2012) 2337–2344.

[7] D. Li, X. Tang, H. Yi, D. Ma, F. Gao, NO_x Removal over Modified Carbon Molecular Sieve Catalysts Using a Combined Adsorption-Discharge Plasma Catalytic Process, Ind. Eng. Chem. Res. 54 (2015) 9097–9103.

[8] A. M. Rubel, J. M. Stencel, Effect of Pressure on NO_x Adsorption by Activated Carbons, Energ Fuel. 10 (1996) 704–708.

[9] Y. Li, Y. Guo, J. Xiong, T. Zhu, J. Hao, The Roles of Sulfur-Containing Species in the Selective Catalytic Reduction of NO with NH_3 over Activated_Carbon, Ind. Eng. Chem. Res. 55 (2016) 12341–12349.

[10] W. Yang, F. Liu, L. Xie, Z. Lian, H. He, Effect of V_2O_5 Additive on the SO_2 Resistance of a Fe_2O_3/AC Catalyst for NH_3-SCR of NO_x at Low Temperatures, Ind. Eng. Chem. Res. 55 (2016) 2677–2685.

[11] H. Wang, Z. Qu, S. Dong, C. Tang, Mechanistic Investigation into the Effect of Sulfuration on the FeW Catalysts for the Selective Catalytic Reduction of NO_x with NH_3, ACS Appl. Mater. Interfaces. 9 (2017) 7017–7028.

[12] J. Liu, J. Liu, Z. Zhao, Y. Wei, W. Song, J. Li, X. Zhang, A Unique Fe/Beta@TiO_2 Core–Shell Catalyst by Small-Grain Molecular Sieve as the Core and TiO_2 Nanosize Thin Film as the Shell for the Removal of NO_x, Ind. Eng. Chem. Res. 56 (2017) 5833–5842.

[13] A. Folli, J. Z. Bloh, K. Armstrong, E. Richards, D. M. Murphy, L. Lu, C. J. Kiely, Morgan, D. J. Ronald, I. Smith, A. C. Mclaughlin, D. E. Macphee, Improving the Selectivity of Photocatalytic NO_x Abatement through Improved O_2 Reduction Pathways Using $Ti_{0.909}W_{0.091}O_2N_x$ Semiconductor Nanoparticles: From Characterization to Photocatalytic Performance, ACS Catal. Articles ASAP (As Soon As Publishable), 6927–6938.

[14] I. Heo, M. K. Kim, S. Sung, I-S. Nam, B. K. Cho, K. L. Olson, W. Li, Combination of Photocatalysis and HC/SCR for Improved Activity and Durability of DeNOx Catalysts, Environ. Sci. Technol. 47 (2013) 3657–3664.

[15] B. Weinberger, D. L. Laskin, D. E. Heck, J. D. Laskin, The Toxicology of Inhaled Nitric Oxide, Toxicol. Sci. 59 (2001) 5–16.

[16] K. Fujiwara, S. E. Pratsinis, Single Pd atoms on TiO_2 dominate photocatalytic NOx removal, Appl. Catal. B-Environ. 226 (2018) 127–134.

[17] J. C. Yu, V. Nguyenb, J. Lasekc, J. C. S. Wu, Titania nanosheet photocatalysts with dominantly exposed (001) reactive facets for photocatalytic NO_x abatement, Appl. Catal. B-Environ. 219 (2017) 391–400.

[18] M. Guo, T. Ling, C. Poon, Photocatalytic NO_x degradation of concrete surface layers intermixed and spray-coated with nano-TiO_2: Influence of experimental factors, Cem. Concr. Compos. 83 (2017) 279–289.

[19] N. H. Nguyen, H. Bai, Photocatalytic removal of NO and NO_2 using titania nanotubes synthesized by hydrothermal method, J. Environ. Sci. 26 (2014) 1180–1187.

[20] A. Tawari, W. Einicke, R. Gläser, Photocatalytic oxidation of no over composites of titanium dioxide and zeolite ZSM-5, Catalysts. 6 (2016) 31.

[21] T. Ibusuki, K. Takeuchi, Removal of low concentration nitrogen-oxides through photoassisted heterogeneous catalysis, J. Mol. Catal. A-Chem. 88 (1994) 93–102.

[22] H. Ichiura, T. Kitaoka, H. Tanaka, Photocatalytic oxidation of NO_x using composite sheets containing TiO_2 and a metal compound, Chemosphere. 51 (2003) 855–860.

[23] N. H. Nguyen, H. Bai, N.H. Nguyen, H. Bai, Effect of washing pH on the properties of titanate nanotubes and its activity for photocatalytic oxidation of NO and NO_2, Appl. Surf. Sci. 355 (2015) 672–680.

[24] C. Guan, X. Li, Y. Luo, Z. Huang, Heterogeneous Reaction of NO_2 on α-Al_2O_3 in the Dark and Simulated Sunlight, J. Phys. Chem. A. 118 (2014) 6999−7006.

[25] L. Sivachandiran, F. Thevenet, A. Rousseauc, D. Bianch, NO_2 adsorption mechanism on TiO_2: An in-situ transmission infrared spectroscopy study, Appl. Catal. B-Environ. 198 (2016) 411–419.

[26] M. M. Kantcheva, V. P. Bushev, K. Hadjiivanov, Nitrogen Dioxide Adsorption on Deuteroxylated Titania (Anatase), J. Chem. Soc.-Faraday Trans. 88 (1992) 3087−3089.

[27] K. Hadjiivanov, H. Knözinger, Species formed after NO adsorption and NO+O_2 co-adsorption on TiO_2: an FTIR spectroscopic study, Phys. Chem. Chem. Phys. 2 (20002) 803–2806.

[28] J. Soria, J. Sanz, I. Sobrados, J. M. Coronado, M. D. Hernández-Alonso, F. Fresno, Water-Hydroxyl Interactions on Small Anatase Nanoparticles Prepared by the Hydrothermal Route, J. Phys. Chem. C. 114 (2010) 16534–16540.

[29] F. Giraud, J. Couble, C. Geantet, N. Guilhaume, E. Puzenat, S. Gros, L. Porcheron, M. Kanniche, D. Bianchi, Experimental Microkinetic Approach of De-NO_x by NH_3 on $V_2O_5/WO_3/TiO_2$ Catalysts. Individual Heats of Adsorption of Adsorbed H_2O Species on Sulfate-Free and Sulfated TiO_2 Supports, J. Phys. Chem. C. 119 (2015) 16089−16105.

[30] W. El-Alami, D. Garzón Sousa, J. M. Díaz González, C. Fernández Rodríguez, O. González Díaz, J. M Doña Rodríguez, M.El Azzouzi, J. Araña, TiO_2 and F-TiO_2 photocatalytic deactivation in gas phase, Chem. Phys. Lett. 684 (2017) 164–170.

[31] T. L. Thompson, J. T. Jr. Yates, Surface science studies of the photoactivation of TiO_2 new photochemical processes, Chem. Rev. 106 (2006) 4428–4453.

[32] M.J. Hernández Rodríguez, E. Pulido Melián, O. González Díaz, J. Araña, M. Macías, A. González Orive, J.M. Doña Rodríguez, Comparison of supported TiO_2 catalysts in the photocatalytic degradation of NO_x, J. Mol. Catal. A-Chem. 413 (2016) 56–66.

[33] Z. Sheng, Z. Wu, Y. Liu, H. Wang, Gas-phase photocatalytic oxidation of NO over palladium modified TiO_2 catalysts, Catal. Commun. 9 (2008) 1941–1944.

[34] D. J. Goebbert, E. Garand, T. Wende, R. Bergamann, G. Meijer, K. R. Asmis, D. M. Neurma, Infrared Spectroscopy of the Microhidated Nitrate Ions NO_3-$(H_2O)_{1-6}$, J. Phys. Chem. A. 113 (2009) 7584–7592.

[35] L. Castoldi, R. Matarrese, S. Morandi, L. Righini, L. Lietti, New insights on the adsorption, thermal decomposition and reduction of NO_x over Pt- and Ba- based catalysts, Appl. Catal. B-Environ. 224 (2018) 249–263.

[36] A. L. Goodman, E. T. Bernard, V. H. Grassian, Spectroscopic Study of Nitric Acid and Water Adsorption on Oxide Particles: Enhanced Nitric Acid Uptake Kinetics in the Presence of Adsorbed Water, J. Phys. Chem. A. 105 (2001) 6443–6457.

[37] M.A. Debeila, N.J. Coville, M.S. Scurrell, G.R. Hearne, The effect of calcination temperature on the adsorption of nitric oxide on Au-TiO_2: Drifts studies, Appl. Catal. A-Gen. 291 (2005) 98–115.

[38] F. R. Rima, K. Nakata, K. Shimazu, M. Osawa, Surface-Enhanced Infrared Absorption Spectroscopic Studies of Adsorbed Nitrate, Nitric Oxide, and Related

Compounds. Formation and Reduction of Adsorbed Nitrite at a Platinum Electrode. J. Phys. Chem. C. 114 (2010) 6011–6018.

[39] H. Lignell, M. E. Varner, B. J. Finlayson-Pitts, B. R. Gerber, Isomerization and ionization of N_2O_4 on model ice and silica surfaces, Chem. Phys. 405 (2012) 52-59.

[40] Z. Gao, Q. Sun, W. M. H. Sachtler, Adsorption complexes of O_2 on Fe/MFI and their role in the catalytic reduction of NO_x, Appl. Catal. B-Environ. 33 (2001) 9–23.

[41] S. R. Q. Long, R. T. Yang, Reaction Mechanism of Selective Catalytic Reduction of NO with NH_3 over Fe-ZSM-5 Catalyst, J. Catal. 207 (2002) 224–231.

[42] B. C. Hixson, J. W. Jordan, E. L. Wagner, H. M. Bevsek, Reaction Products and Kinetics of the Reaction of NO_2 with γ-Fe_2O_3, J. Phys. Chem. A. 115 (2011) 13364–13369.

[43] M. A. Kamboures, J. D. Raff, Y. Miller, L. F. Phillips, B. J. Finlayson-Pitts, R. Benny Gerber, Complexes of HNO_3 and NO_3^- with NO_2 and N_2O_4, and their potential role in atmospheric HONO formation, Phys. Chem. Chem. Phys. 10 (2008) 6019–6032.

[44] K. Hadjiivanov, V. Avreyska, D. Klissurski, T. Marinova, Surface Species Formed after NO Adsorption and NO + O_2 Coadsorption on ZrO_2 and Sulfated ZrO_2: An FTIR Spectroscopic Study, Langmuir. 18 (2002) 1619–1625.

[45] A. A. Davydov, Y. A. Lokhov, Y. M. Shchekochikhin, Study of nitrogen oxide interaction with a Cr_2O_3 surface with IR spectroscopy, Kinet. Katal. (in Russian); Kinet. Catal. (English translation), 19 (1978) 673–680.

[46] A. Davydov, Molecular Spectroscopy of Oxide Catalyst Surfaces, John Wiley & Sons, Ltd, 2003.

[47] A. Desikusumastuti, T. Staudt, M. Happel, M. Laurin, J. Libuda, Adsorption and reaction of NO_2 on ordered alumina films and mixed baria–alumina nanoparticles: Cooperative versus non-cooperative reactionmechanisms, J. Catal. 260 (2008) 315–328.

[48] O. Marie, N. Malicki, C. Pommier, P. Massiani, A. Vos, R. Schoonheydt, P. Geerlings, C. Henriques, F. Thibault-Starzyk, NO_2 disproportionation for the IR characterisation of basic zeolites, Chem. Commun. (2005) 1049–1051.

[49] J. Hot, T. Martinez, B. Wayser, E. Ringot1, A. Bertron. Photocatalytic degradation of NO/NO_2 gas injected into a 10-m^3 experimental chamber, Environ. Sci. Pollut. Res. (2017) 12562–12570.

[50] C. Pazé, G. Gubitosa, S. O. Giacone, G. Spoto, F. X. Llabrés i Xamena, A. Zecchina, An XRD, FTIR and TPD Investigation of NO_2 Surface Adsorption Sites of δ, γ-Al_2O_3 and Barium Supported δ, γ-Al_2O_3, Top. Catal. 30 (2004) 169−175.

[51] D. A. Syomin, B. J. Finlayson-Pitts, HONO decomposition on borosilicate glass surfaces: implications for environmental chamber studies and field experiments, Phys. Chem. Chem. Phys. 5 (2003) 5236–5242.

[52] A. Mills, L. Burns, C. O'Rourke, S. Elouali, Kinetics of the photocatalysed oxidation of NO in the ISO 22197 reactor, J. Photochem. Photobiol. A-Chem. 321 (2016) 137–142.

[53] Y. Ohko, Y. Nakamura, A. Fukuda, S. Matsuzawa, K. Takeuchi, Photocatalytic Oxidation of Nitrogen Dioxide with TiO_2 Thin Films under Continuous UV-Light Illumination, J. Phys. Chem. C, 112 (2008) 10502–10508.

[54] A. El Zein, Y. Bedjanian, Interaction of NO_2 with TiO_2 surface under UV irradiation: measurements of the uptake coefficient, Atmos. Chem. Phys. 12 (2012) 1013–1020.

[55] A. Tawari, W. Einicke, R. Gläser, Photocatalytic Oxidation of NO over Composites of Titanium Dioxide and Zeolite ZSM-5, Catalysts. 6 (2016) 31.

[56] S. Laufs, J. Kleffmann, Investigations on HONO formation from photolysis of adsorbed HNO_3 on quartz glass surfaces, Phys.Chem.Chem.Phys. 18 (2016) 9616.

[57] M. Mochida, B. J. Finlayson-Pitts, FTIR Studies of the Reaction of Gaseous NO with HNO_3 on Porous Glass: Implications for Conversion of HNO_3 to Photochemically Active NO_x in the Atmosphere, J. Phys. Chem. A. 104 (2000) 9705–9711.

[58] N. A. Saliba, H. Yang, B. J. Finlayson-Pitts, Reaction of Gaseous Nitric Oxide with Nitric Acid on Silica Surfaces in the Presence of Water at Room Temperature, J. Phys. Chem. A. 105 (2001) 10339–10346.

[59] R. Dillert, A. Engel, J. Große, P. Lindner, D. W. Bahnemann, Light intensity dependence of the kinetics of the photocatalytic oxidation of nitrogen(II) oxide at the surface of TiO_2, Phys. Chem. Chem. Phys. 15 (2013) 20876–20886.

[60] C. E. Richeson, P. Mulder, V. W. Bowry, K. U. Ingold, The Complex Chemistry of Peroxynitrite Decomposition: New Insights, J. Am. Chem. Soc. 120 (1998) 7211–7219.

[61] H. Tsukahara, T. Ishida, M. Mayumi, Gas-Phase Oxidation of Nitric Oxide: Chemical Kinetics and Rate Constant, Nitric Oxide: Biol. Chem. 3 (1999) 191 -198.

[62] O. B. Gadzhiev, S. K. Ignatov, A. G. Razuvaev, A. E. Masunov, Quantum Chemical Study of Trimolecular Reaction Mechanism between Nitric Oxide and Oxygen in the Gas Phase, J. Phys. Chem. A 113 (2009) 9092–9101.

[63] J. Zawadzki, M. Wis´niewski, K. Skowron´ska, Heterogeneous reactions of NO and NO–O on the surface of Carbons, Carbon 41 (2003) 235–246.

Acknowledgements

We are grateful for the financial support of the Spanish Ministry of Economy and Competitiveness through the projects CTQ2015-64664-C2-1-P and IPT-2012-0927-420000 (HORMIFOT). We would also like to thank the Canary Islands Agency for Research, Innovation and the Information Society (ACIISI) of the Canary Islands Government for its funding through the FANOX Project (PROID2017010034) and the Spanish Ministry of Science and Innovation for the UNLP10-3E-726 infrastructure, co-financed with ERDF funds. D. Garzón Sousa would also like to thank the University of Las Palmas de Gran Canaria for its funding through the PhD Grant Program.

Figure captions

Figure 1. Reaction system

Figure 2. FTIR spectra of the P25 and HT-ET.

Figure 3. (% NO_{conv}) vs. reaction time. (Determination error ± 1.9 % maximum).

Figure 4. Cumulative selectivity of all the NO converted at each reaction time to NO_2.

Figure 5. FTIR spectra of the P25 and HT-ET after 18 h of NO adsorption in darkness.

Figure 6. FTIR spectra obtained during the photocatalytic conversion of NO with the P25 (A) and the HT-ET (B) at 0, 1, 2 and 18 hours of reaction time.

Figure 7. Evolution of the bands obtained with the HT-ET (during the NO conversion studies after 18 h) in an air-only atmosphere.

Figure 8. NO_2 moles eliminated during adsorption of NO_2, $\left(NO_2\right)_{ads}$, NO_x moles eliminated during photocatalytic conversion of NO_2, $\left(NO_x\right)_{NO_2-phot}$, and photocatalytic conversion of NO, $\left(NO_x\right)_{NO-phot}$. (Determination error ± 7 µmol/g maximum)

Figure 9. $\left(NO\right)_{disprop\rightarrow NO_2}$ (black), $\left[\left(NO\right)_{disprop\rightarrow NO_2}\times 3\right]$ (red), and $\left(NO_2\right)_{ads}-\left[\left(NO\right)_{disprop\rightarrow NO_2}\times 3\right]$ (blue), P25 (A) and HT-ET (B). (Determination error ± 7 µmol·g^{-1} maximum)

Figure 10. FTIR spectra obtained after 18 h of NO_2 adsorption, NO_2 photocatalytic conversion and NO photocatalytic conversion with the P25 (A) and HT-ET (B).

Figure 11. NO_2 formed during HNO_3 photolysis (A) and reaction of the HNO_3/NO_3^--H^+ adsorbed on the P25 with NO in darkness (B). (Determination error ± 40 µmol/g).

Figure 12. FTIR spectra of: a) HNO_3 adsorbed on P25; b) HNO_3 adsorbed on P25 + NO during 2 h; c) the sample after b) in atmosphere without NO during 12 h; d) HNO_3 adsorbed on P25 + NO_2 during 2 h; and e) the sample after d) in atmosphere without NO during 12 h.

Figure 13. Global scheme of the photocatalytic conversion of NO.

Table caption

Table 1. Crystalline phases and surface area of catalysts studied.

Table

Catalyst	Anatase %	Rutile %	Surface area ($m^2 \cdot g^{-1}$)
P25	80	20	50 ± 1.5
HT-ET	100	-	167 ± 5

Table 1.

Figure

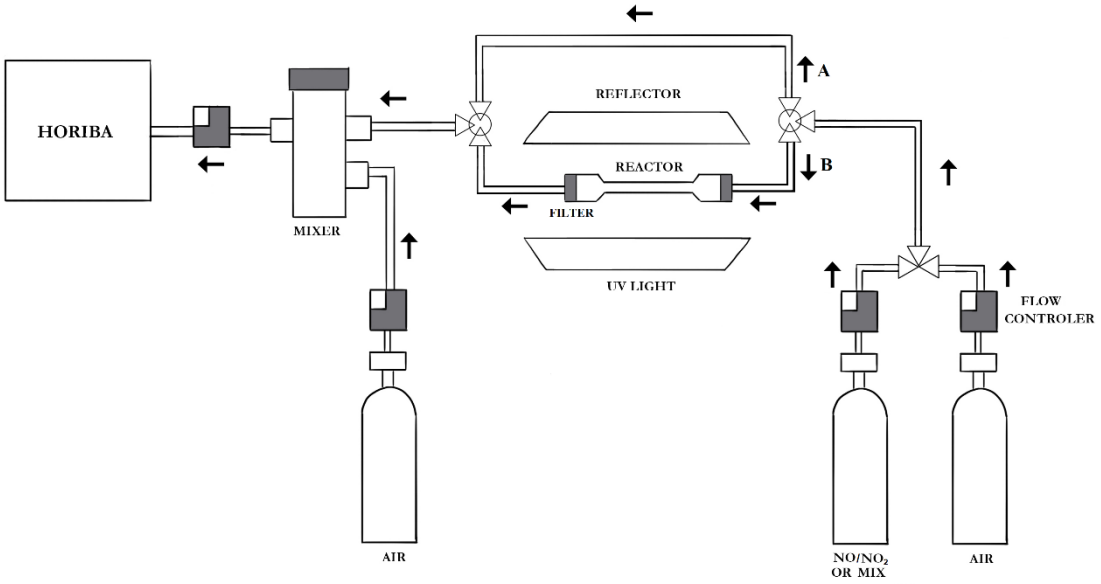

Figure 1.

Figure

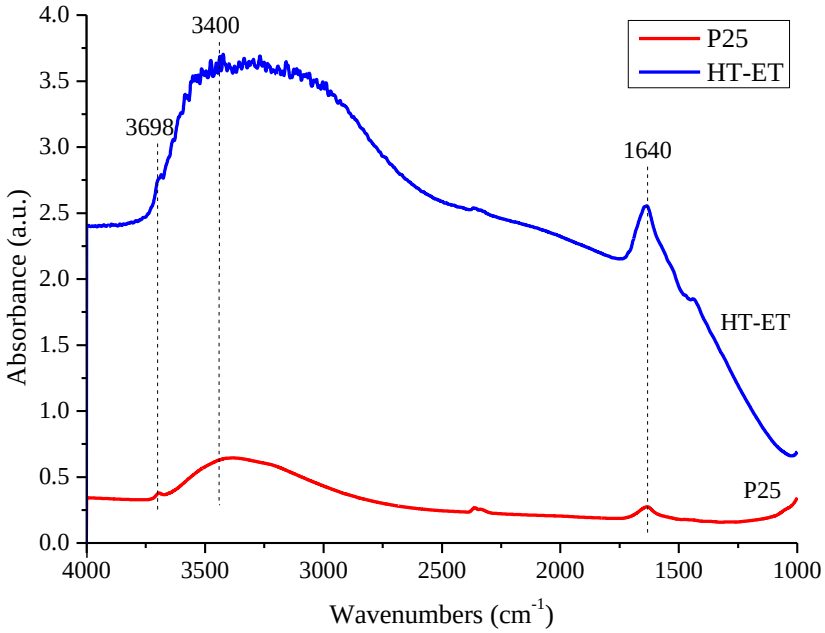

Figure 2.

Figure

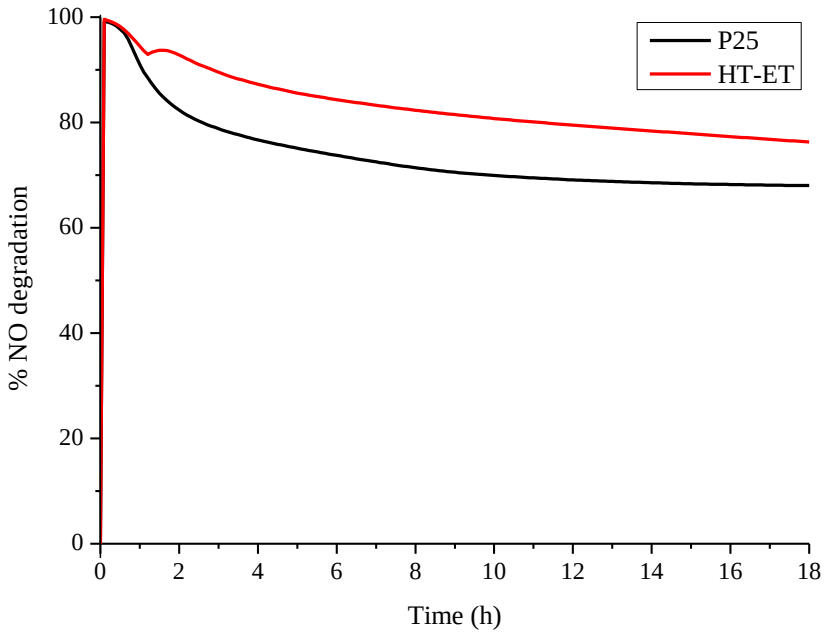

Figure 3.

Figure

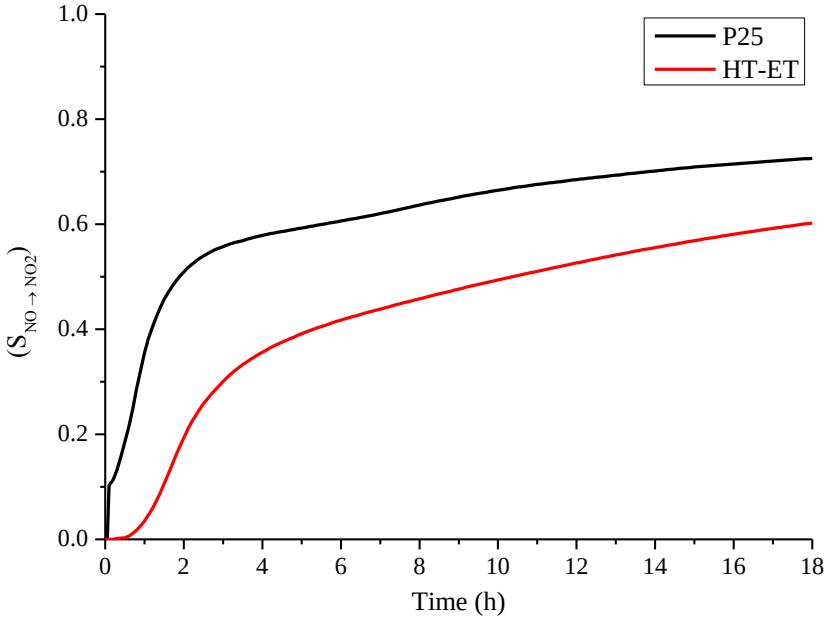

Figure 4.

Figure

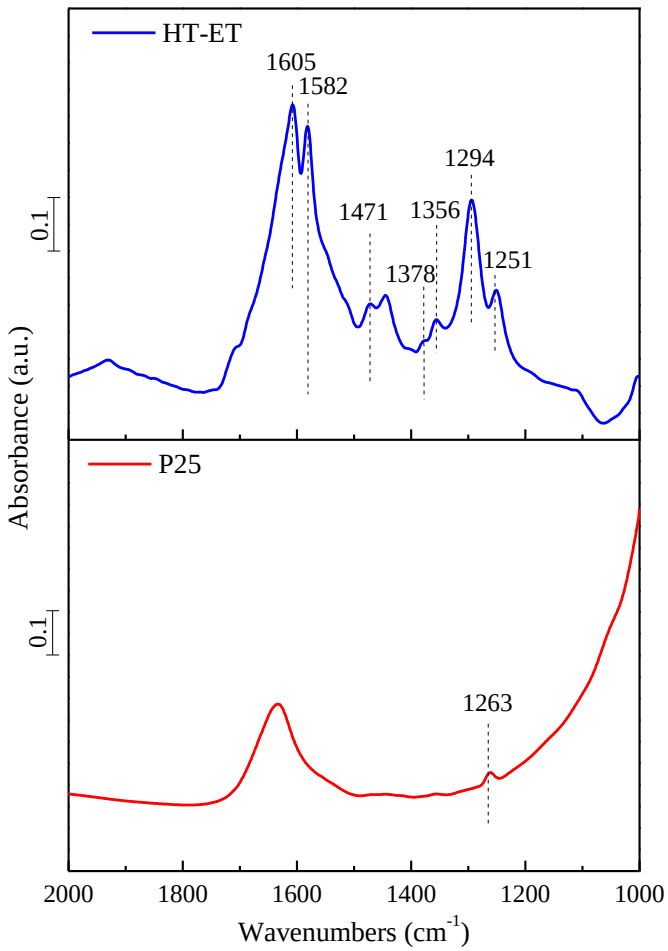

Figure 5.

Figure

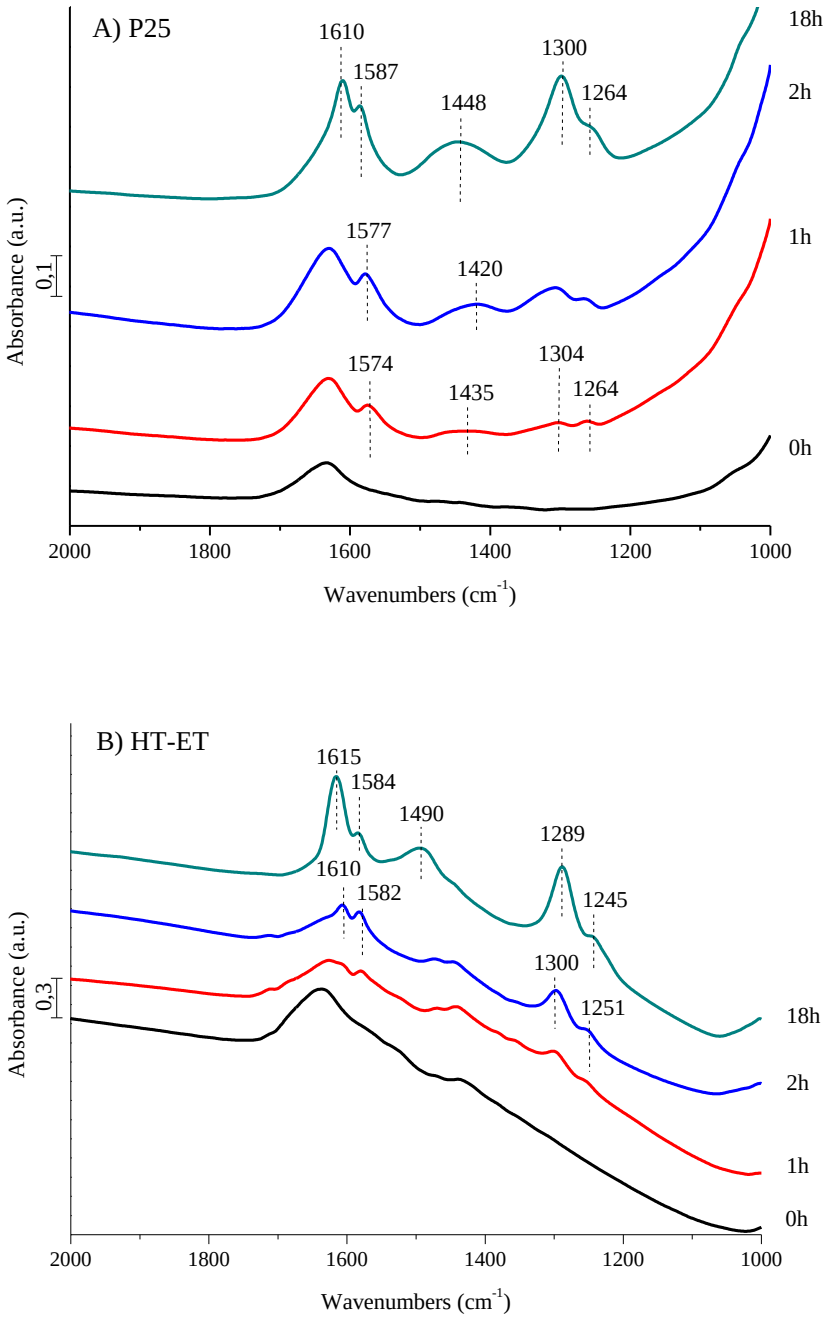

Figure 6.

Figure

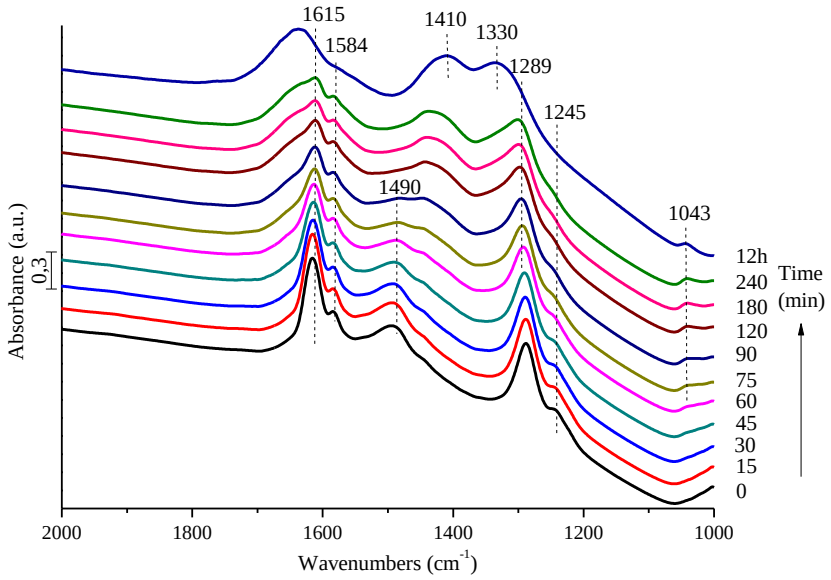

Figure 7.

Figure

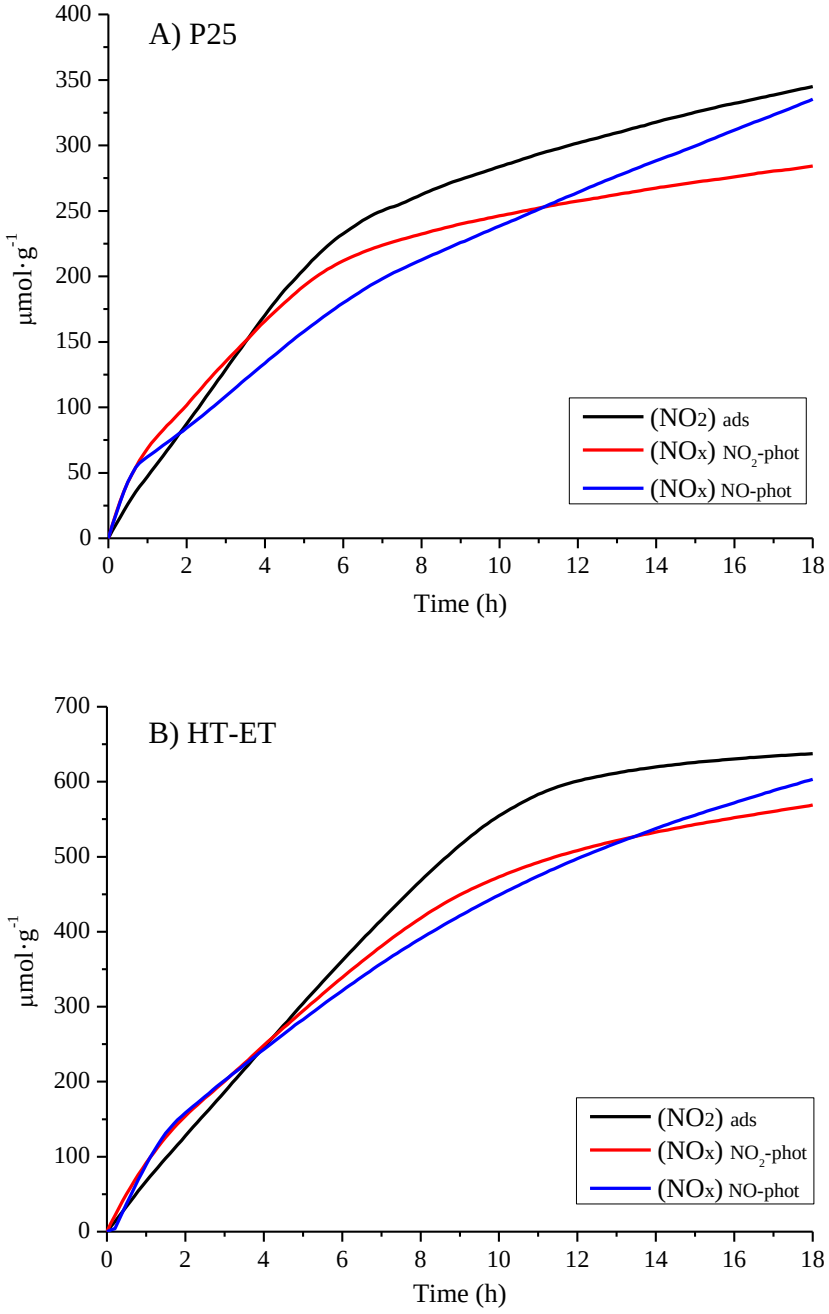

Figure 8.

Figure

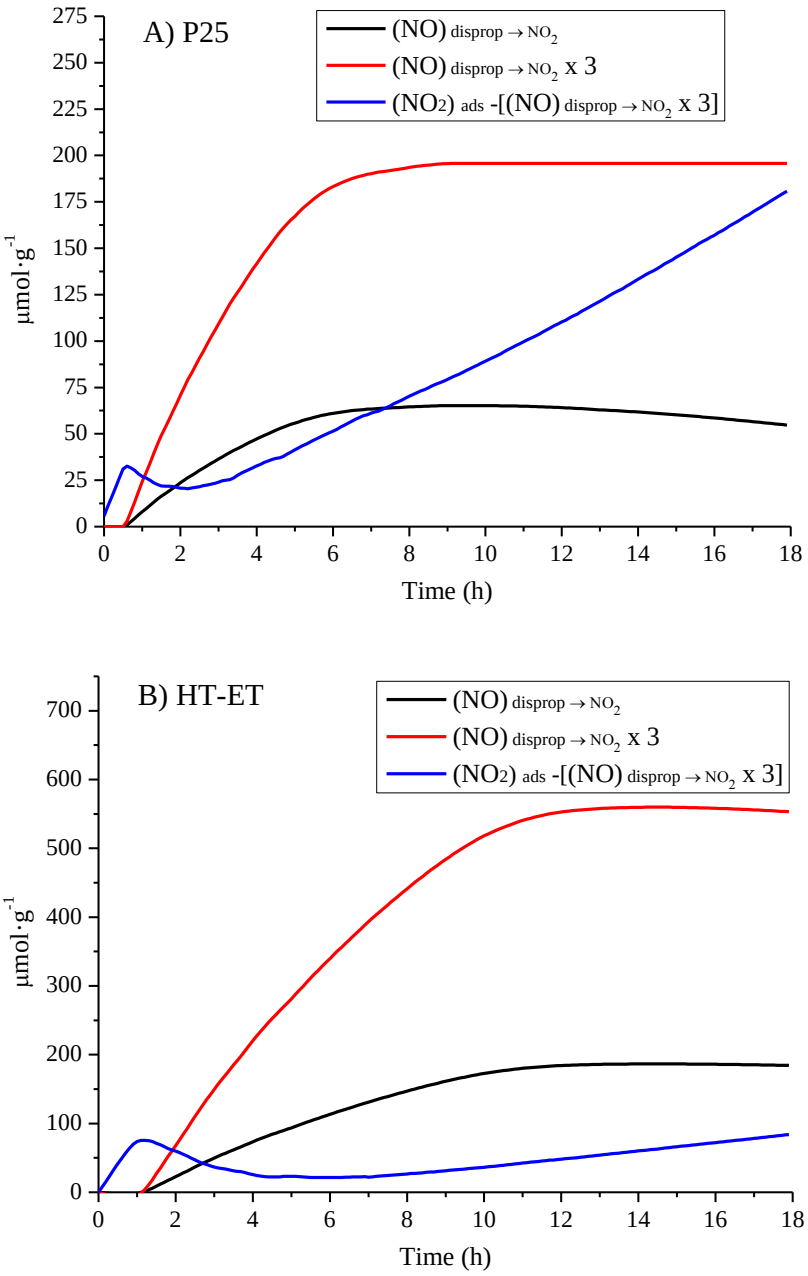

Figure 9

Figure

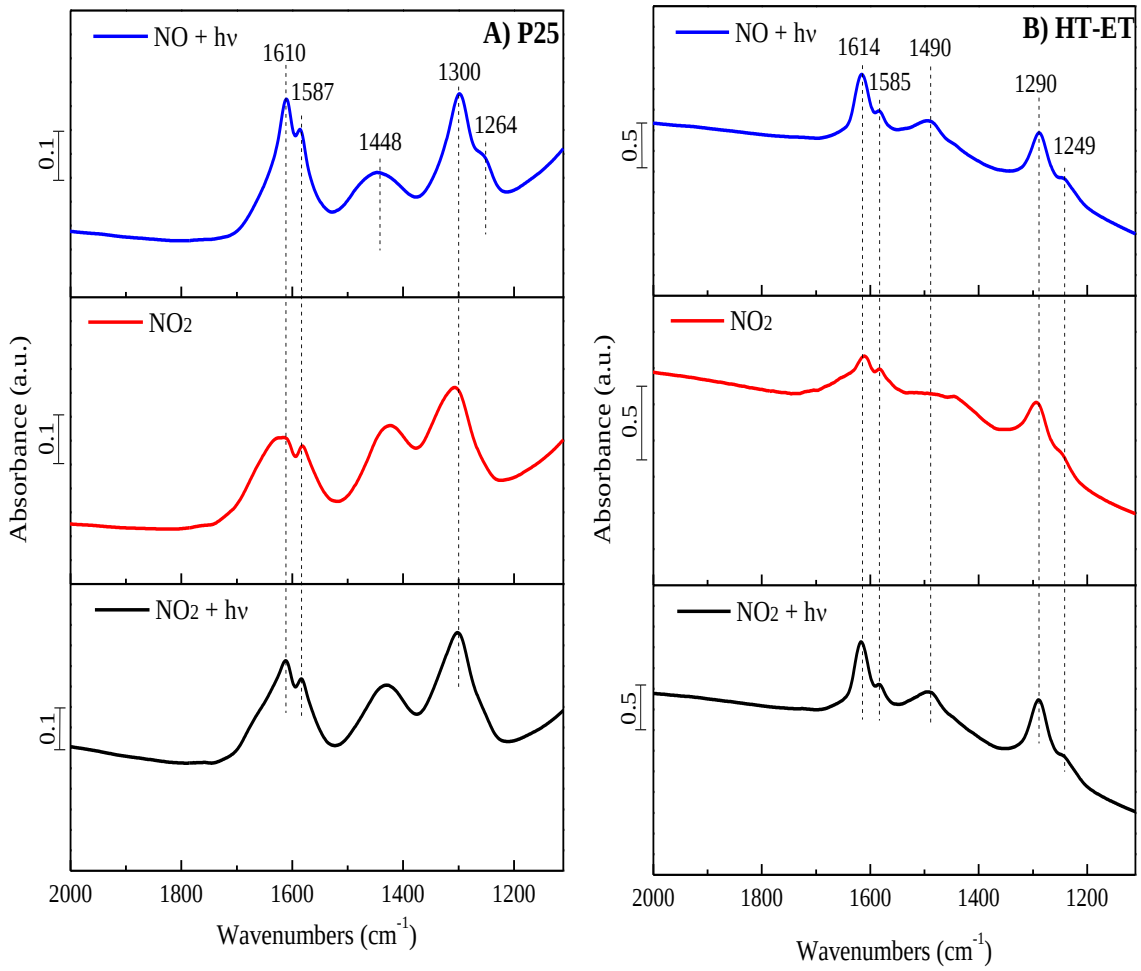

Figure 10.

Figure

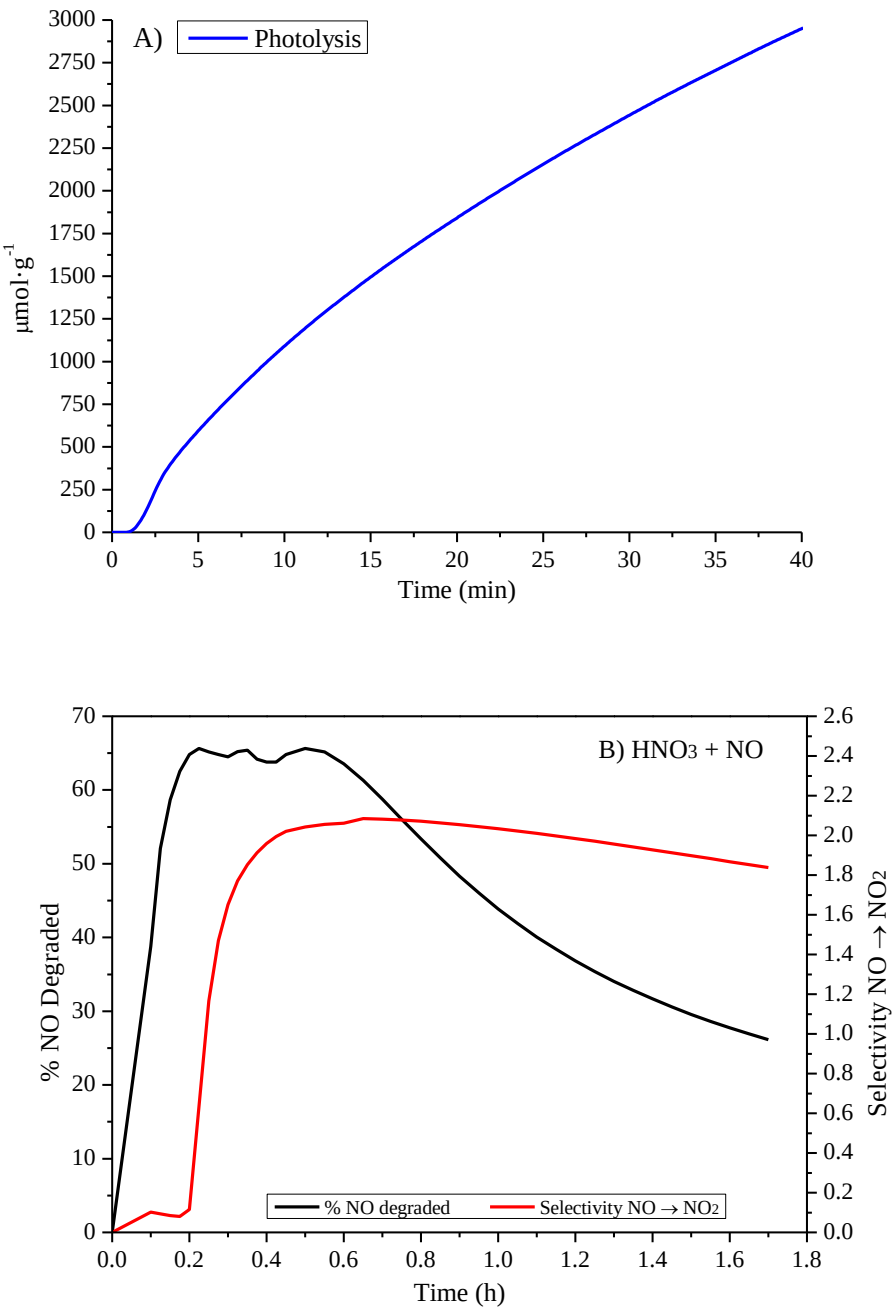

Figure 11.

Figure

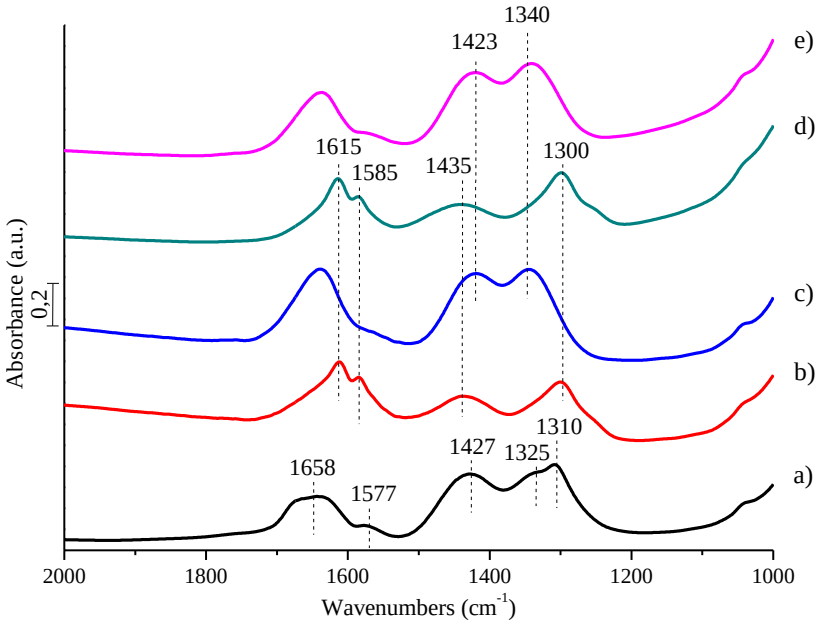

Figure 12.

Figure

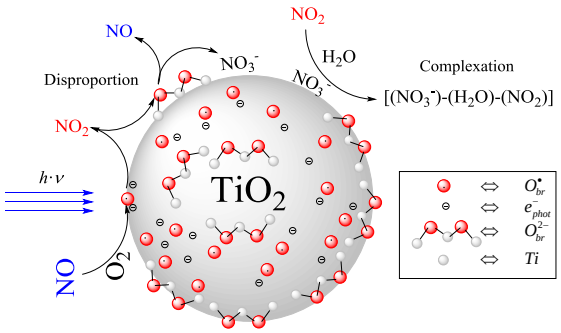

Figure 13.